A distributed simple dynamical systems approach (dS2 v1.0) for computationally efficient hydrological modelling

Joost Buitink[1], Lieke A. Melsen[1], James W. Kirchner[2, 3, 4], and Adriaan J. Teuling[1]

[1]Hydrology and Quantitative Water Management Group, Wageningen University, Wageningen, The Netherlands
[2]Department of Environmental Systems Science, ETH Zurich, Zurich, 8092, Switzerland
[3]Swiss Federal Research Institute WSL, Birmensdorf, 8903, Switzerland
[4]Department of Earth and Planetary Science, University of California, Berkeley, California, 94720, USA

Correspondence: Joost Buitink (joost.buitink@wur.nl)

Abstract. In this paper, we introduce a new numerically robust distributed rainfall runoff model for computationally efficiency simulation at high (hourly) temporal resolution: the distributed simple dynamical systems (dS2) model. The model is based on the simple dynamical systems approach as proposed by Kirchner (2009), and the distributed implementation allows for spatial heterogeneity in the parameters and/or model forcing fields for instance as derived from precipitation radar data. The concept

5   is extended with snow and routing modules, where the latter transports water from each pixel to the catchment outlet. The sensitivity function, which links changes in storage to changes in discharge, is implemented by a new 3-parameter equation that is able to represent the widely observed downward curvature in log-log space. The simplicity of the underlying concept allows the model to calculate discharge in a computationally efficient manner, even at high temporal and spatial resolution, while maintaining proven model performance at high temporal and spatial resolution. The model code is written in Python in

10 order to be easily readable and adjustable while maintaining computational efficiency. Since this model has short run times, it allows for extended sensitivity and uncertainty studies with relatively low computational costs. A test application shows a good and constant model performance across scales ranging from 3 to over 1700 km^2.

1 Introduction

Hydrological models are essential tools for applications ranging from sensitivity analysis to impact assessment and forecasting.

15 Generally, the aim of rainfall-runoff models is to simulate streamflow given a precipitation time series. Depending on factors such as the research aim and the climatological/geological setting, different model structures or process representation might be preferred. This, in combination with the inherent complexity and heterogeneity of (sub)surface hydrological processes, has lead to the development of numerous different hydrological models over the past decades, each with their own focus. Examples of such rainfall-runoff models and modelling tools include, amongst many others: SWAT (Arnold et al., 1998), HBV

20 (Lindström et al., 1997), TOPMODEL (Beven and Kirkby, 1979), VIC (Liang et al., 1994, 1996), SPHY (Terink et al., 2015), FUSE (Clark et al., 2008), SUMMA (Clark et al., 2015), PCR-GLOBWB (Sutanudjaja et al., 2018) and WALRUS (Brauer et al., 2014). Although there is an ongoing debate about whether the hydrological modelling community should move towards

a community model (Weiler and Beven, 2015), different models representing a wide range of complexity and different process representations might be necessary to adequately characterise uncertainty.

Hydrological models are often classified from more conceptual to more process-based models. Conceptual models have fewer processes explicitly parameterized, and as a result their limited number of parameters makes them easier to calibrate. In conceptual models, catchments are often represented by a series of buckets or storages, which mimic processes with different response times. Their typical scale of application is that of small to medium (mesoscale) catchments, generally in a lumped fashion. Process-based models, on the other hand, contain a much higher number of parameters. These models are often applied in a distributed fashion, where many of the parameter values are based on maps of vegetation and soil properties. However, often conceptual parameters remain that require calibration or tweaking. Even though process-based models should give a better representation of the physical reality, many models can easily be beaten in performance by a simple neural network (Abramowitz, 2005), or model results can be reproduced without much loss of accuracy by models with a much lower number of parameters (Koster and Suarez, 2001; Best et al., 2015; Liu et al., 2018).

Whereas conceptual models often perform satisfactory at the daily resolution at the lumped basin scale, they lack the ability to explicitly simulate spatially distributed processes that might be needed to accurately predict streamflow response at larger scales. In a study over a large number of basins in France, Lobligeois et al. (2014) found that (hourly) model performance markedly increased from the (lumped) basin-scale to a resolution of around 10 km^2 when using aggregated radar precipitation as model input. Other studies (e.g. Ruiz-Villanueva et al., 2012) have also highlighted the importance of spatial variability of rainfall, in particular the movement of storms with respect to the channel network, for flash flood simulation. Another example of a spatially distributed process that affects streamflow is the melting of snow that can depend both on elevation (via temperature) and aspect (via radiation). Comola et al. (2015), for example, showed that aspect needs to be considered for accurate simulation of snowmelt and runoff dynamics in mesoscale catchments. The spatial organization of the stream network within a basin also affects the response to rainfall, as has been shown by studies based on the catchment width function or the Geomorphological Instantaneous Unit Hydrograph (Kirkby, 1976; Rodríguez-Iturbe and Valdes, 1979).

The need to improve spatially explicit information in hydrological models aligns with the increasing availability of high-resolution continental-scale forcing datasets. These include for instance merged radar data (Huuskonen et al., 2013), interpolated station data (Cornes et al., 2018), or atmospheric reanalysis (Albergel et al., 2018). There is a growing need for easy-to-apply models that can utilize the potential of spatially distributed input data.

Conceptual models have been applied in a (semi-)distributed manner to account for spatially distributed input data: a lumped model is applied for each individual grid cell, and water is most often transferred to the outlet as a post-processing function. This is, however, not necessarily the most computationally efficient way to deal with spatially distributed data, but rather the result of historical developments. Whereas increased computational power has driven the application of distributed models at increasingly fine (spatial) resolution (Melsen et al., 2016b), it also lead to new challenges: Many aspects of distributed modelling, such as uncertainty estimation and (spatial) parameter estimation, require a high number of runs which further increases the computational demand. An efficient distributed conceptual model to tackle these kind of issues is currently lacking.

An example of a conceptual model that, in spite of its extreme simplicity, has shown a good performance for discharge simulation at the scale of smaller catchments is the simple dynamical systems (SDS) approach introduced by Kirchner (2009). This concept is based on the assumption that discharge is solely dependent on the total amount of stored water in a catchment. It translates changes in storage to changes in discharge using a discharge sensitivity function, without describing internal

5 catchment processes. This sensitivity function is typically parameterized by a 2-parameter power-law, however several studies have suggested a more complex downward-curving rather than linear behaviour in double-logarithmic space (Kirchner, 2009; Teuling et al., 2010; Adamovic et al., 2015). Moreover, the system parameters can be inferred from streamflow recession analysis and potentially from hillslope characteristics (Troch et al., 2003), potentially removing the need for model calibration (Melsen et al., 2014). The model simplicity has the important advantages that discharge can be simulated based on a single

10 equation which can easily be vectorized for distributed implementation, and since storage and discharge are directly linked via the discharge sensitivity function they don't need to be stored separately thus reducing the number of model output fields. In the original test in the humid Plynlimon catchments (area 8.70 and 10.55 km^2), Kirchner (2009) found Nash-Sutcliffe Efficiencies (NSE's) exceeding 0.95 during the model validation when calibrating model parameters, and efficiencies exceeding 0.90 when parameters were obtained from recession analysis. Others have also found the concept to work well in less humid catchments.

15 Teuling et al. (2010) found the method to generally work well in the small (3.3 km^2) Swiss Rietholzbach catchment. Although the method can be expected to work best in hilly catchments, Brauer et al. (2013) found the model to produce reasonable efficiencies after calibration in the small (6.5 km^2) Dutch Hupsel Brook catchment. Adamovic et al. (2015) reported NSE values exceeding 0.6 for most years in several Ardechian catchments in the order of 10–100 km^2. Given the simplicity and good performance of the simple dynamical systems approach at the spatial (order 10 km^2) and temporal (1 h) resolution required for

20 optimal simulation of rainfall-runoff processes in larger (mesoscale) catchments, combining it with simple representations of routing and snowmelt should result in a model that satisfies the required criteria outlined in the previous paragraphs.

Here, we present a flexible and computationally efficient distributed implementation and extension of the simple dynamical systems approach that can be used to investigate spatially distributed hydrological processes in a flexible and efficient manner: the distributed simple dynamical systems (dS2) model. Our aim was to create a model that is able to computationally efficient

25 simulate mesoscale basins at high temporal and spatial resolutions, but also to develop a model code that is easy to use, read and modify. Therefore, the model is written in Python, sacrificing some calculation efficiency. In this model, the catchment is divided into smaller sections using a regular grid, and discharge is simulated according to the SDS approach for each pixel. This distributed implementation allows the concept to be applied to bigger catchments, and also allows for spatial heterogeneity, both in the forcing and in the parameters. Since the original concept consists essentially of only one differential equation, it can

30 be applied in a computationally efficient fashion, vectorizing all cells in the catchment. Snow and routing modules are added to the model to allow for application in snow-dominated regions, and to transport the water from each pixel to the catchment outlet via the drainage network. This efficient distributed implementation lowers the computational burden for high spatial and/or temporal resolution studies, and opens doors for extensive uncertainty studies. We will first introduce the model concept and describe the technical application. Then we discuss the parameter sensitivity and finally, we show an application of the

35 model.

Geoscientific
Model Development
Discussions

2 Model concept

2.1 Simple dynamical systems approach

The simple dynamical systems approach proposed by Kirchner (2009) combines the conservation-of-mass equation with the assumption that discharge is solely dependent on the total storage (excluding snow and ice) in the area of interest:

$$\frac{\mathrm{d}S}{\mathrm{d}t} = P - E - Q, \tag{1}$$

$$Q = f(S), \tag{2}$$

where S represent the total storage, P the precipitation, E the (actual) evaporation and Q the discharge. Differentiating Eq. (2) and combining with Eq. (1) results in the following equation:

$$\frac{\mathrm{d}Q}{\mathrm{d}t} = \frac{\mathrm{d}Q}{\mathrm{d}S}\frac{\mathrm{d}S}{\mathrm{d}t} = \frac{\mathrm{d}Q}{\mathrm{d}S}(P - E - Q) = g(Q)(P - E - Q), \tag{3}$$

where we define $\frac{\mathrm{d}Q}{\mathrm{d}S}$ as the sensitivity function $g(Q)$, describing the sensitivity of discharge to changes in storage. We introduce an evaporation reduction parameter ϵ, which acts as a simple translation from potential to actual evaporation ($E_{\mathrm{act}} = \epsilon \cdot E_{\mathrm{pot}}$). Note that the evaporation here represents the actual evaporation as the concept does not directly allow for evaporation reduction as result of e.g. soil moisture stress. A simple evaporation switch is added, which is described in Section 3.2.

Originally, the SDS approach was introduced as a lumped approach to simulate discharge in small catchments of approximately 10 km^2 (Kirchner, 2009). Several studies have applied this concept to other catchments in Europe (Teuling et al., 2010; Krier et al., 2012; Brauer et al., 2013; Melsen et al., 2014; Adamovic et al., 2015). Some of the catchments in these studies had a size similar to the original scale from Kirchner (2009), yet it was also applied to catchments up to 1000 km^2 in size. One could argue whether the concept is still valid at a scale so different from the scale for which it was initially developed (Beven, 1989, 2001; Sivapalan, 2006; McDonnell et al., 2007), and whether a single sensitivity function is sufficient to capture the spatial complexity of substantially larger basins. In regions with high spatial heterogeneity, grid-based models are likely to yield more realistic results than lumped models (Lobligeois et al., 2014).

To respect the original scale of development and to capture spatial variability, we have developed a distributed implementation of the simple dynamical systems approach. Our distributed implementation builds on the original concept as proposed by Kirchner (2009), and extends this concept with simple snow and routing modules. For the distributed implementation, we assume that the SDS approach is valid for each pixel of a rectangular grid. By defining pixels with a size corresponding to the original scale (in the order of 1 km^2), the scale of application remains similar to the original scale, and both the forcing and the model parameters can be defined for each individual pixel (see Figure 1). In this distributed implementation, we allow precipitation to fall as snow, see Section 2.3. We added a routing module to transport water from each pixel to the river outlet, by adding a time delay to each pixel based on the distance to the outlet and a travel speed parameter, see Section 2.4. The model can be run with different choices for Δt, yet in order to respect the spatio-temporal resolution the default time step is one hour. This model has been built with a focus on computational efficiency, meaning that all grid cells in the catchment are stored in a single vector, allowing for vectorized computations (see Fig. 1b). This results in a matrix with the rows and columns
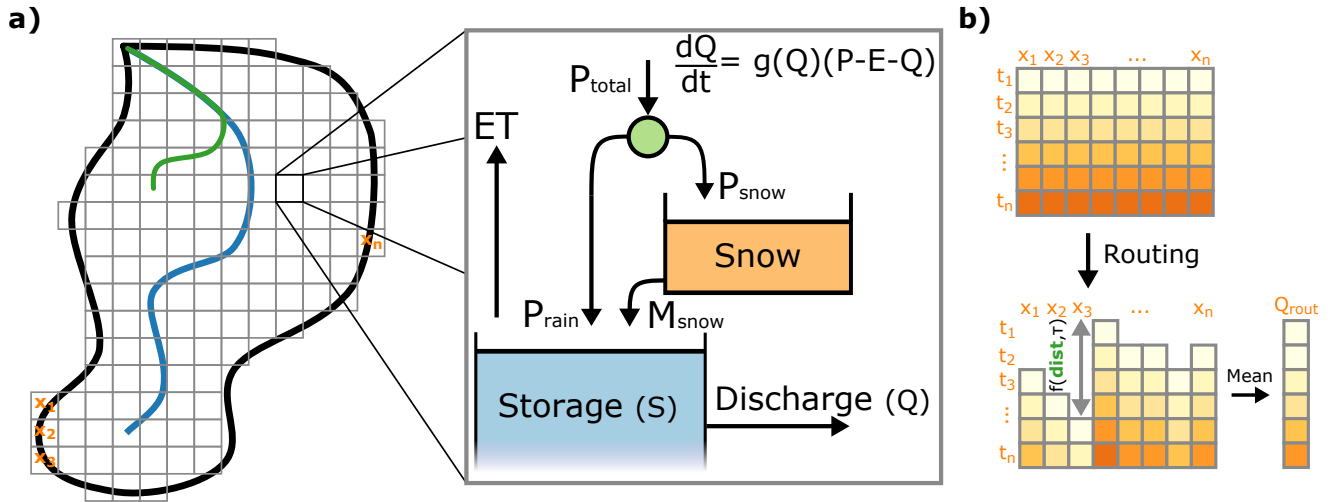
Figure 1. Efficient distributed implementation of the simple dynamical systems approach, which is solved for each pixel. The left hand side of panel a represents a catchment, with a regular grid covering the catchment area. The green line indicates the flow path on which the routing lag is based (green "dist" in panel b). Panel b shows how the catchment is translated to a matrix to allow for computationally efficient calculations, and how the matrix is modified in the routing algorithm, by shifting each column based on the distance to the outlet and the routing parameter τ.

indicating time and space, respectively. As a result, the routing conceptualization is a modification of this matrix, where each column is shifted to induce a temporal delay.

2.2 Discharge sensitivity

As previously mentioned, the sensitivity function is required to translate changes in storage to changes in discharge. This
5 function can have any shape. Kirchner (2009) originally presented a simple power-law version of this sensitivity function for purposes of illustration:

$$g(Q) = \frac{\mathrm{d}Q}{\mathrm{d}S} = aQ^b,$$ (4)

where a and b define the slope and intersect of the sensitivity function in log-log space. This power-law relation has been widely used in experimental and theoretical studies (e.g. Troch et al., 1993; Brutsaert and Lopez, 1998; Tague and Grant, 2004;
10 Rupp and Selker, 2006; Lyon and Troch, 2007; Rupp and Woods, 2008). This relatively simple sensitivity function allows the

translation of discharge into storage, using the following equation:

$$\int \mathrm{d}S = \int \frac{\mathrm{d}Q}{g(Q)}, \tag{5}$$

$$S(Q) = \begin{cases} \dfrac{1}{a}\dfrac{1}{1-b}Q^{1-b} + S_0, & b \neq 1 \\ \dfrac{1}{a}\ln(Q) + S_0, & b = 1, \end{cases} \tag{6}$$

where S_0 is the integration constant, meaning that only relative storage changes can be obtained using this method. The value

5 of b affects the meaning of S_0, as described by Kirchner (2009). However, most catchments show recession behaviour that differs from a power-law relation between $\mathrm{d}Q/\mathrm{d}S$ and Q (Kirchner, 2009; Teuling et al., 2010; Krier et al., 2012; Adamovic et al., 2015). Therefore, a more complex formulation of the sensitivity function was also proposed by Kirchner (2009):

$$\ln(g(Q)) = c_1 + c_2\ln(Q) + c_3(\ln(Q))^2, \tag{7}$$

where c_1, c_2 and c_3 are the three parameters of this quadratic equation. This quadratic equation allows for a concave relation

10 between the recession rate and the discharge in log-log space. This equation has one downside, however: since it is shaped like a parabola in log-log space, there is always an optimum in the discharge sensitivity. This implies that with an increasing Q, the system becomes less sensitive at some point. This behaviour is unrealistic and unwanted when performing automatic calibration or random parameter sampling runs. Therefore, we have added an additional term to the original power-law equation, which accounts for the concave shape of the sensitivity function:

15 $$g(Q) = aQ^b \cdot \mathrm{e}^{\gamma/Q}, \tag{8}$$

where a, b and γ are the three parameters describing the shape of the discharge sensitivity. However, we have rewritten this equation to include all parameters in the exponent term, as this improves computational efficiency:

$$g(Q) = \mathrm{e}^{\alpha + \beta \cdot \ln(Q) + \gamma/Q}, \tag{9}$$

with $\alpha = \ln(a)$ and $\beta = b$ from the Eq. (8). In Fig. 2, the effect of each parameter on the shape of the sensitivity function is

20 presented. Discharge observations from Teuling et al. (2010) are also included to indicate the importance of the γ parameter. This equation has the benefit that it can be rewritten to the original power law equation, if $\gamma = 0$:

$$g(Q) = \mathrm{e}^{\alpha + \beta \cdot \ln(Q)} = \mathrm{e}^{\alpha} \cdot Q^{\beta}, \tag{10}$$

where $a = \mathrm{e}^{\alpha}$ and $b = \beta$ from Eq. (4). This concept allows us to use parameters from previous studies, and to transform the discharge time series to a storage time series according to Eq. (5). A disadvantage of this new sensitivity function is that, due

25 to the addition of the γ/Q term, there is no longer an analytical solution, but the equation can still be integrated numerically.

2.3 Snow processes

In our distributed implementation, we allow precipitation to fall as snow. Snow is treated as a separate storage (see Fig. 1a), where snowmelt is added to the simple dynamical systems approach in the form of liquid precipitation, following the
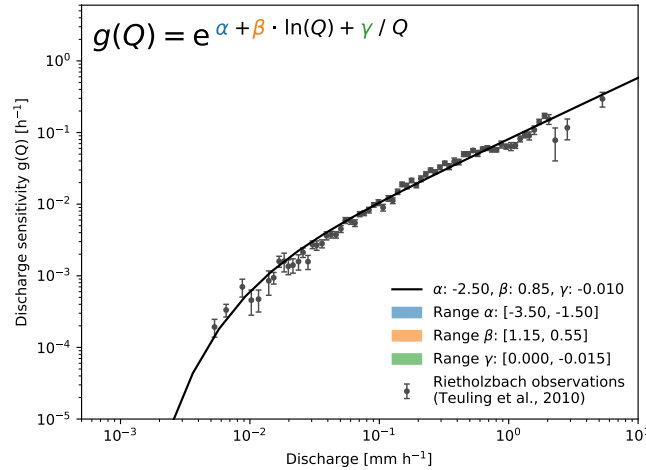
Figure 2. Parameterization of the discharge sensitivity, including the effects of the three parameters. α affects the intercept, β affects the slope and γ affects the curvature at low discharge values. Parameter values for each parameter are given in the legend as their min-max range.

methodology of Teuling et al. (2010). We assume snowmelt to be dependent on both temperature and radiation, following the restricted degree-day radiation balance approach (Kustas et al., 1994). The snow storage is conceptualized based on the following equations:

$$\frac{\mathrm{d}S_{\mathrm{snow}}}{\mathrm{d}t} = P_{\mathrm{snow}} - M_{\mathrm{snow}}, \tag{11}$$

$$P_{\mathrm{snow}} = \begin{cases} P_{\mathrm{total}} & \text{if } T <= T_0 \\ 0 & \text{if } T > T_0, \end{cases} \tag{12}$$

$$M_{\mathrm{snow}} = \begin{cases} ddf \cdot (T - T_0) + rdf \cdot R_{\mathrm{g}} & \text{if } M_{\mathrm{snow}} \cdot \Delta t <= S_{\mathrm{snow}} \\ \dfrac{S_{\mathrm{snow}}}{\Delta t} & \text{if } M_{\mathrm{snow}} \cdot \Delta t > S_{\mathrm{snow}}, \end{cases} \tag{13}$$

where S_{snow} is the total snow storage in mm, P_{snow} the precipitation falling as snow in mm h^{-1}, M_{snow} is the snowmelt in mm h^{-1}, T is the air temperature in °C, T_0 is the critical temperature for snowmelt °C, ddf is the degree-day factor mm h^{-1} °C^{-1}, rdf is the conversion factor for energy flux density to snowmelt depth in mm h^{-1} (W m^{-2})$^{-1}$, R_{g} is the global radiation in W m^{-2}, and Δt is the time step in hours. If no radiation observations are available, the snowmelt equation is modified to the normal degree-day method.

In Fig. 3, the effect of this snow conceptualization is presented using synthetic forcing data. In this figure, one can see that radiation can cause snow to melt even when temperatures are still below the critical temperature (0°C in this example). If the temperature exceeds this threshold, radiation amplifies the melting of snow, resulting in an earlier depletion of the snow storage. Finally, if snow processes are not relevant in the region of interest, the snow conceptualization can be turned off to further reduce the computational demand (see the dashed line in Fig. 3 for the resulting discharge simulation).
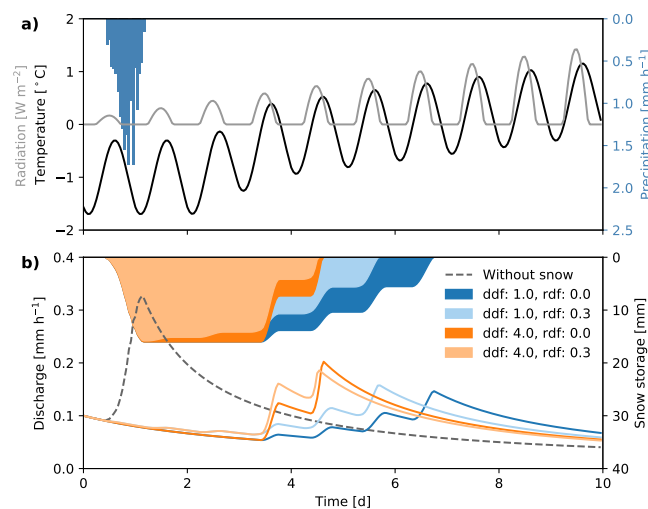
Figure 3. Simulation results with and without the snow conceptualization. Top panel shows the model input, bottom panel shows the model output. The four hydrographs represent runs with different snow parameter values (see legend, in mm h^{-1}). We fixed the critical temperature T_0 to 0°C. To visualize the influence of the different parameters, we used unrealistically high ddf and rdf values.

2.4 Flow routing

A simple efficient routing conceptualization was added to the distributed model to transport water from each grid cell to the outlet of the catchment. In most studies applying the simple dynamical systems approach, a constant delay factor was added to the generated runoff time series, in order to account for the delay caused by the river network. Since our distributed

5   implementation has pixels at distinct different locations, we need to account for attenuation caused by the river network. The routing concept presented here is based on the width function (Kirkby, 1976), where we assume that the stream network applies a temporal delay proportional to the distance to the outlet. This distance is combined with the travel speed parameter (τ) to determine the lag time for each pixel (see the green line and shifting of columns in Fig. 1). An example of this concept is presented in Fig. 4a.

10   The width function in Fig. 4a reflects the shape and stream network of a synthetic catchment. The distance of each pixel can be translated to a time delay using the travel speed parameter τ. This delay is in discrete steps (see Fig. 4b), determined by the time step of the model. Lower flow speed values result in larger time delays, and vice versa. The hydrograph in Fig. 4c shows that peaks are more attenuated with lower flow speed values. In this example, we assume homogeneous precipitation across the entire catchment, but in reality, the heterogeneity of precipitation events also influences how the discharge peak is attenuated.

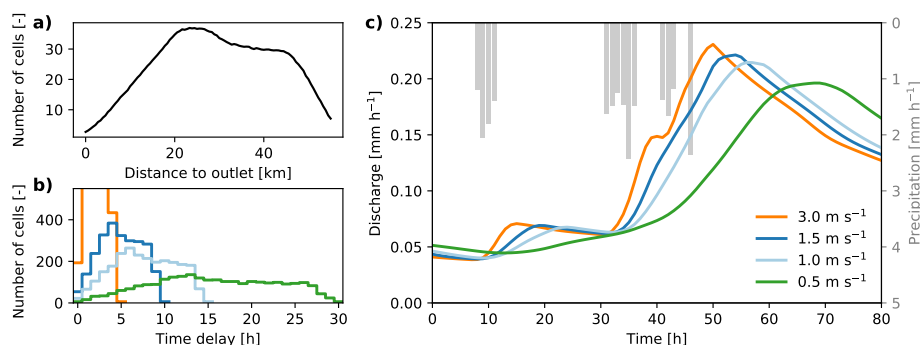15   This concept does not include diffusion of a flood wave, but only incorporates advection.

Figure 4. The routing concept visualized: a) the width function of a synthetic catchment, b) the corresponding travel speed given four different τ values, and c) the effect of different τ values on the hydrograph.

3 Technical aspects

3.1 Model implementation

One of the main aims of this model was computational efficiency. Low-level languages generally perform faster calculations, but this comes at the price of user-friendliness and ease-of-use. The model implementation is focussed on efficiency, but

5 some calculation time is sacrificed for a higher-level but more user friendly language. The model is written in Python 3.6 and largely utilizes the Numpy library. The efficient implementation of arrays in Numpy allows for fast computations over entire arrays. Due to the simplicity of the simple dynamical systems approach, we need to solve only one equation (besides the snow conceptualization). Numpy allows functions to be vectorized: receiving and outputting an array of values, while applying the same function on each individual value. This is computationally more efficient than the step-by-step application of the same

10 function to each element in the array.

To get an idea of the computational efficiency of the model, example run times are presented in Fig. 5. We ran the model for 3 months at an hourly time step using synthetic forcing data for a wide range of model cells, reflecting different catchment sizes or model resolutions, to get an idea how the computational demand scales with catchment size or resolution. We separated the time spent in the numerical solver, the IO operations, and the routing module. In the IO operations, we include reading the

15 settings file, reading the input data, and writing the model results. The grey bars in Fig. 5 represent the "traditional" modelling approach, where the numerical solver is called for each individual pixel and time step. This extra for-loop drastically increases runtimes by a factor of more than 10 (this is also a property of Python, being an interpreted language instead of a compiled language). Simulating Europe for three months at hourly time steps and at a resolution of 5×5 km^2 (roughly $2^{18.6}$ pixels) would take approximately 5 minutes with the efficient dS2 model, demonstrating the enormous potential of this model to

20 explore uncertainty and spatial patterns in parameters. The runtimes show a small inconsistency in the increase of runtimes with the increase in pixels. This is most likely the result of an internal Python or Numpy threshold. The current version of dS2 does not yet support automatic multi-threading, which is expected to even further reduce runtimes, especially in large basins.
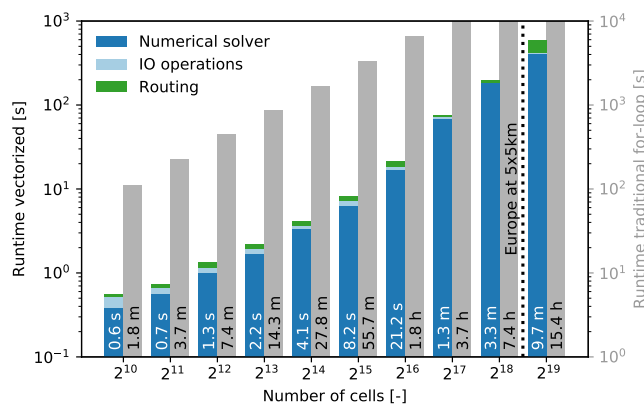
Figure 5. Runtimes for a simulation of three months with an hourly time step with varying number of pixels, ran on a single core of a normal desktop (Intel Core i7-6700, 16GB RAM). The grey bars represent model run times where the numerical solver is called for each individual pixel, and are keyed to the right hand scale, making the difference in runtimes appear smaller than it really is. The dotted line represents the number of pixels when simulating Europe at 5×5 km^2 resolution.

When applying the model to very large basins and/or running for very long periods, the random access memory (RAM) can become a limiting factor, as storing data in the RAM is by far most efficient. To prevent exceeding the RAM, the user can define the maximum amount of RAM the model is allowed to use, and dS2 will chunk the input and output data accordingly. For example, running the model for a basin with 1500 pixels for a period of 4 years on an hourly time step would require

5 approximately 800MB. Additionally, to reduce the time spent with reading and writing the files on the disk, we rely on a special data format: Numpy memmap. This data file directly maps arrays to the hard drive without storing any metadata, to ensure fast reading and writing. The downside is that this format does not have any metadata, meaning the shape and data type needs to be known prior to reading the file. In order to store the model output in a more common format, the model can transform the Numpy memmap data to the more commonly used NetCDF format, including meta-data.

10 **3.2 Adaptive time stepping**

Since this concept allows for non-linear reservoirs, the simulated response can vary over several orders of magnitude within a single time step. This non-linearity can cause numerical errors, which can be prevented by reducing the time step. Several options are available, where the Cash-Karp method is the typical textbook approach to explicitly solving differential equations (Cash and Karp, 1990). This method is based on the Runge-Kutta scheme, and uses the difference between fourth and fifth

15 order estimations to measure the potential numerical error. This can be used to reduce the time step if the difference exceeds a certain threshold. However, to ensure optimal computational efficiency, we decided to incorporate the knowledge about the differential equation (Eq. (3)) to determine whether time step reduction is necessary. We have implemented the explicit fourth order Runge-Kutta (RK4) scheme, with an adaptive time stepping scheme. We have identified cases where the RK4 scheme
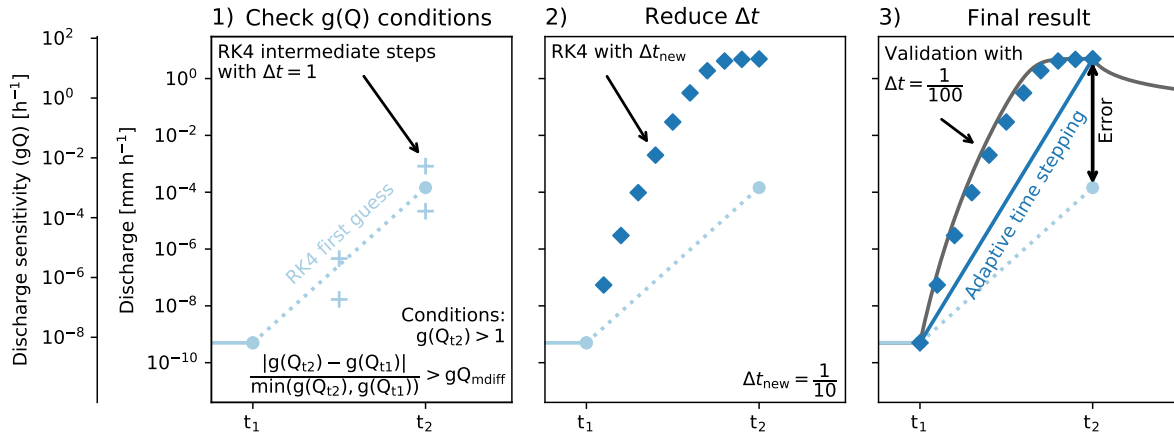
Figure 6. Three steps in the adaptive time stepping scheme. Note that in extreme cases, both Q and $g(Q)$ can change over several orders of magnitude between t_1 and t_2. The error represents the numerical error without the adaptive time stepping scheme.

can become numerically unstable, and used these cases to reduce the internal time step. These cases are explained in more detail below. This adaptive time stepping scheme is visualized in Fig. 6.

The adaptive time stepping scheme operates in three steps. In the first step, the discharge for the next time step is calculated using the explicit Runge-Kutta 4 scheme. For both time steps, the discharge sensitivities are calculated based on the following

5   equation:

$$gQ_{\mathrm{diff}} = \frac{|g(Q)_{\mathrm{t2}} - g(Q)_{\mathrm{t1}}|}{\min(g(Q)_{\mathrm{t2}} - g(Q)_{\mathrm{t1}})}, \tag{14}$$

where the numerator represents the absolute difference between the two discharge sensitivities, and the denominator the lowest discharge sensitivity to ensure the comparison also works during the falling limb of the hydrograph. The time step will be reduced whenever at least one of two conditions are met: (1) when $g(Q_{\mathrm{t2}}) \cdot \Delta t > 1$, or (2) when gQ_{diff} exceeds a certain

10   threshold (gQ_{mdiff}). The first condition requires a smaller time step, since values of $g(Q) \cdot \Delta t > 1$ indicate that the system is extremely sensitive, and that a smaller time step is required to optimally account for this sensitivity. For this condition, the time step is reduced according to the following equation:

$$\frac{\Delta t}{\Delta t_{\mathrm{new}}} = \max(5, \min(g(Q_{\mathrm{t2}}) \cdot 10, 50)), \tag{15}$$

where the reduction in Δt is dependent on the size of $g(Q_{\mathrm{t2}})$. We defined a lower and upper limit to the time step reduction,

15   to ensure the solver gains enough precision but does not spend too much time on a single time step. Both values can be changed by the user. The second condition is triggered when $g(Q)$ covers several orders of magnitude in a single time step. A threshold gQ_{diff} is defined, describing how many times $g(Q_{\mathrm{t2}})$ is allowed to deviate from $g(Q_{\mathrm{t1}})$. If this threshold is exceeded ($gQ_{\mathrm{diff}} > gQ_{\mathrm{mdiff}}$), a smaller time step is required since RK4 is not able to accurately solve the differential equation over this

many orders of magnitude. The resulting reduced time step is based on the following equation:

$$\frac{\Delta t}{\Delta t_{\text{new}}} = \max(5, \min(gQ_{\text{diff}}^{dt\_reduction}, 50)),$$ (16)

where the reduction in Δt is dependent on the difference between $g(Q_{t1})$ and $g(Q_{t2})$, raised to the power $dt\_reduction$, and the same lower and upper limit to the time step reduction are used. The RK4 scheme is used over these reduced time steps,

5   until the original time step is reached. This final value is saved as output, and the intermediate steps are discarded. In Fig. 6 step 3, we validate the adaptive time stepping scheme with an even finer time step ($\frac{1}{100}$) which we assume to approach the analytical solution, and we conclude that the adaptive time stepping scheme yields reliable results. This figure shows that the adaptive time stepping scheme avoided a large numerical error (the difference between the two solutions: $Q_{t2} \approx 10^0$ mm h^{-1} vs $Q_{t2} \approx 10^{-4}$ mm h^{-1}).

10   During periods with low discharge and relatively high evaporation, the numerical solver can result in negative discharge amounts. To prevent this from happening, we define a threshold for discharge, below which no evaporation is allowed to occur. This mimics evaporation reduction during periods with low storage volumes, as discharge and storage are directly linked. For the pixels where the discharge is below this threshold, the evaporation rate is set to 0 mm h^{-1}. The value of the discharge threshold is currently set at 10^{-4} mm h^{-1}, but can be altered by the user. All model parameters are presented in Table A1.

15   **3.3   Closure of the water balance**

The concept of this model is based on the water balance, yet it does not explicitly solve the water balance as most hydrological models do. The water balance is indirectly solved by calculating changes in storage. To check whether the model still respects the water balance, the closure of the water balance is calculated using the following equation:

$$wbal\_error = P_t - E_t - \int_{t-1}^{t} Q - \Delta S,$$ (17)

20           $$\Delta S = S(Q_t) - S(Q_{t-1}),$$ (18)

where $wbal\_error$ is the error in the water balance for each time step t, which ideally should result in a value of zero. The change in storage can be calculated using the storage at the beginning and at the end of the time step. The integral over Q indicates that one needs to consider the volume of water that is discharged during the time step. This depends on how the variables are considered in time within the model. Figure 7a explains how the different fluxes are positioned within the model.

25   The model assumes that the precipitation and evaporation values are summations of the entire duration of a single time step. The resulting discharge values are, however, only representative at the end of the time step, and not a summation over the time step. Due to the strong non-linearity of the system, the total volume of water discharged during a single time step cannot be represented by the discharge at the end of the time step, as indicated by the dotted red line in Fig. 7a.

To estimate the volume of water discharged during the time step, one needs a discharge value that is representative for the

30   volume of water discharged during that time step. The easiest way to calculate this, it to take the average of the discharges at time step t and $t-1$. However, if the sensitivity function is strongly non-linear, the average discharge might not be representative
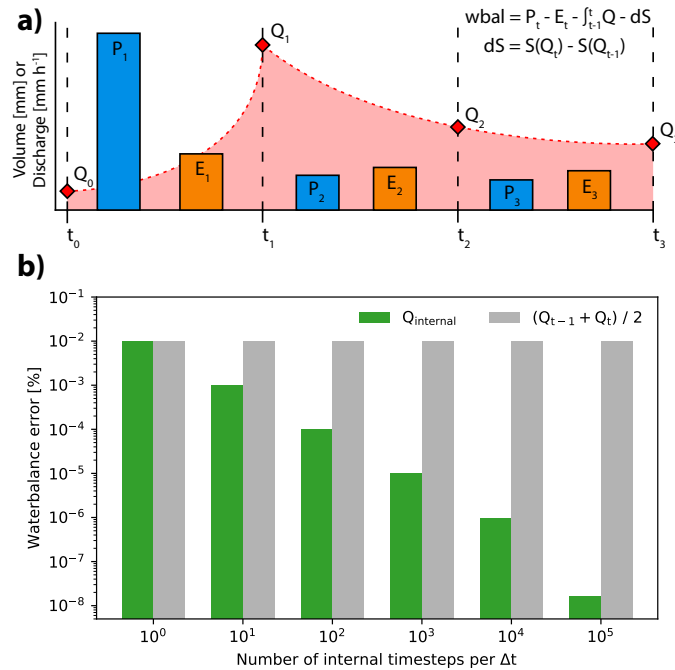
Figure 7. Closure of the water balance per time step. Panel a shows the timing of the different variables. Red area under the dotted line indicates the total volume of water discharged per time step. Panel b shows the average absolute error in the water balance per timestep with different internal time steps, where the error is defined as the percentage of the total precipitation during the simulation period.

for the volume of water discharged during that time step. To improve the volume estimation, one can subdivide each time step, and base the volume estimation on the mean discharge of the resulting shorter steps. This comparison is shown in Fig 7b. The gray bars represent the error in the water balance when the total discharge volume is estimated using the discharge averaged over time steps t and $t - 1$. This error does not reduce with an increase in internal time steps, as the discharge prediction at t

5 changes only marginally. However, if the total discharge volume is estimated using the discharge at each internal time step, the total error in the water balance is reduced from $10^{-2}\%$ to $10^{-8}\%$. This indicates that the model concept is able to successfully close the water balance, given that the discharge volume per time step is accurately accounted for. Please note that this example is to show that the concept successfully closes the water balance, but the current version of the model only outputs discharge at the end of the time step.

4 Parameter sensitivity

10

We investigated the response of the model to each parameter by plotting the response surface over realistic parameter ranges. The results of this analysis are presented in Fig. 8. We selected the Kling-Gupta efficiency (KGE) as the performance metric. We created a synthetic time series of observations that has parameters that are in the middle of each subplot, which are used
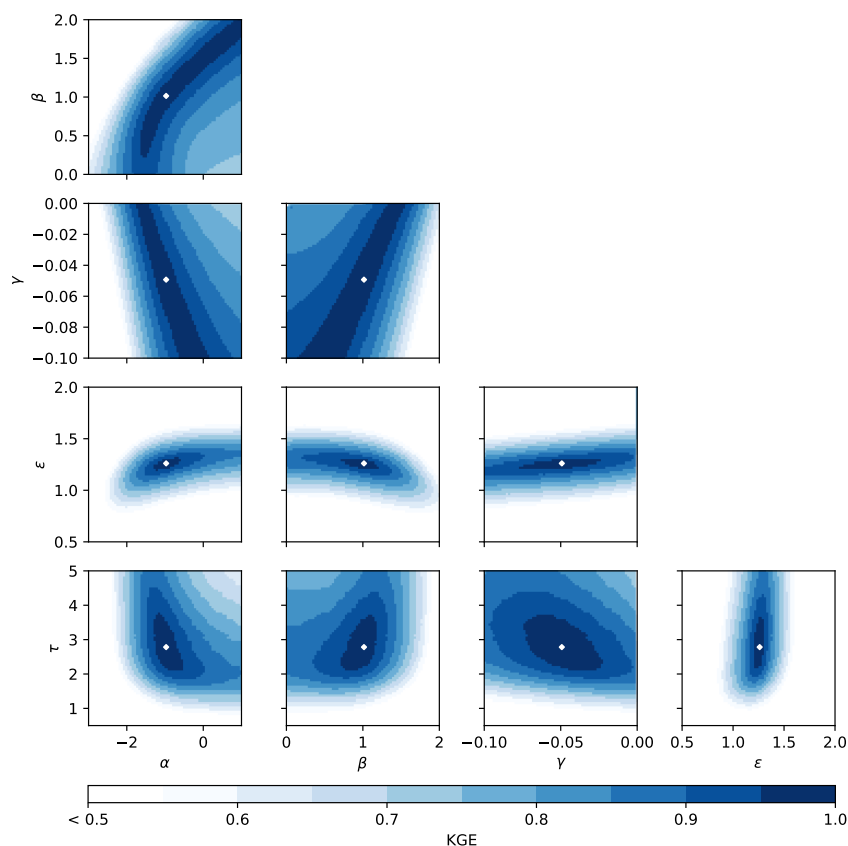
Figure 8. Response surface plots with the Kling-Gupta efficiency (KGE) as the performance metric for a synthetic experiment. The white dot in the middle of each graph represents the location where KGE is equal to 1. Each plot consists of 4900 model runs – where the model has 200 cells, ran for one year on hourly timestep – and took 1 hour and 15 minutes to run on a normal desktop (Intel Core i7-6700, 16GB RAM).

to calculate the KGE. It is striking that the three $g(Q)$ parameters show large regions with similar model performance, and seem to be correlated, which Melsen et al. (2014) also showed for the α and β parameters for a lumped application. However, based on the theoretical considerations (Troch et al., 1993; Brutsaert and Lopez, 1998; Tague and Grant, 2004; Rupp and Selker, 2006; Lyon and Troch, 2007; Rupp and Woods, 2008, e.g.), we can conclude that at least the α and β parameters are required to optimally capture the discharge sensitivity, and based on other studies using the simple dynamical systems approach (Kirchner, 2009; Teuling et al., 2010; Krier et al., 2012; Adamovic et al., 2015), that a third parameter (γ in this case) is required to capture the curvature in the $g(Q)$ relation. These response surface graphs indicate that local optimization algorithms might struggle to find the global maximum due to the large equifinality regions. We therefore recommend not to use a single parameter combination, but rather to use multiple parameter sets to account for equifinality
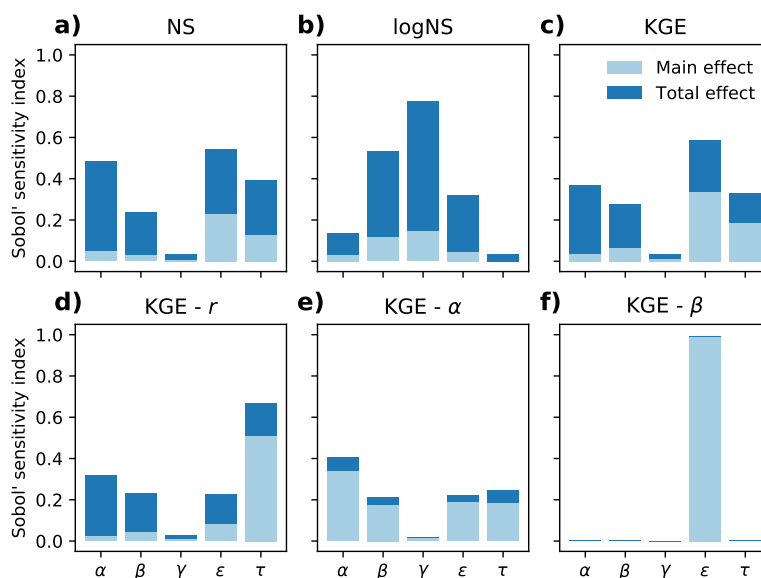
Figure 9. Sobol' parameter sensitivity for a synthetic experiment, shown for different performance statistics. The bottom row (panels d to f) show the three components of the Kling-Gupta efficiency: Pearson correlation coefficient (KGE - r), ratio of variability (KGE - α) and bias (KGE - β).

Furthermore, we also analysed the parameter sensitivity according to Sobol' (2001), Saltelli (2002), and Saltelli et al. (2010). The global sensitivity analysis method is designed to analyse the sensitivity to different performance statistics to each parameter. Sobol' sensitivity analysis creates a set of $n \cdot (2k + 2)$ combinations, where k is the number of parameters, and n is the number of samples that sample the parameter space. For this study, we chose a sample of $1,000$, and focused on the five main parameters (α, β, γ, ϵ, τ) resulting in $12,000$ parameter sets. Usually, this is a rather computationally expensive method, but due to the computational efficiency of this model, we were able to run all parameter sets in just under 6 hours (model with 100 cells, simulation period of 2 years on hourly time step, on a normal desktop with an Intel Core i7-6700 and 16GB RAM). The parameter boundaries were set to the same values as used in the response surface plots. For each parameter combination, multiple performance statistics were calculated. Next, Sobol' sensitivity analysis is able to extract the influence of each parameter on the variation in the performance statistic caused only by that parameter ("main effect"), and the influence of the parameter including all variance caused by interactions with other parameters ("total effect") (Sobol', 2001; Saltelli, 2002; Saltelli et al., 2010). The results from the analysis are presented in Fig. 9.

It is clearly visible that parameter sensitivity depends on the performance metric used. The Nash-Sutcliffe and Kling-Gupta efficiencies show roughly the same response, as is expected. Nash-Sutcliffe calculated on the logarithmic discharge values shows a very different response, with γ being one of the most sensitive parameters. This is in line with our expectations, as the γ parameter describes the downward curvature of the $g(Q)$ function, where it mostly affects the lower discharge volumes. As a result, this parameter is not very prominently visible in the NS and KGE sensitivity plots, since these metrics tend to put

more focus on higher discharges. These graphs also show that there are some parameter correlations influencing the results. This was already visible in Fig. 8, where we see correlations between the three $g(Q)$ parameters.

The most interesting patterns are visible in the bottom three subplots, where the three components of the KGE are presented. The correlation coefficient (r, Fig. 9d) is most sensitive for the routing parameter τ, since this parameter essentially deals with

5 the timing of discharge peaks. The ratio of variability (α, Fig. 9e) does not show a single parameter to be most important, yet all parameters show some degree of sensitivity. For the bias (β, Fig. 9f), the evaporation parameter ϵ is by far the most sensitive parameter, since it determines the total volume of water that evaporates and thus the total volume of discharge. All other parameters can only control either the response of discharge to precipitation or the timing of the peaks. Since the roles of the parameters ϵ and τ are relatively clearly defined, predominantly affecting the bias and correlation, respectively, we hypothesize

10 that this information can be used for more efficient optimization procedures by reducing the number of dimensions. One could optimize the ϵ parameter only on the bias of the simulations, followed by an optimization of the τ parameter on the correlation. Finally, the three $g(Q)$ parameters can be optimized on either the ratio of variability or the total Kling-Gupta efficiency. This reduces the optimization from a 5-dimensional space to two 1-dimensional problems and a single 3-dimensional problem.

5   Example application

15 In this section, we apply the model to the Thur, a mesoscale basin (1700 km^2) in the Swiss Alps. This basin was selected since it contains many measurement locations, where the catchment used by Teuling et al. (2010) is one of the sub-basins. Since Teuling et al. (2010) showed that the concept is able to simulate the discharge at small scale, we take this opportunity to see how the model performs at different spatial extents. The model was applied at a 1 km^2 resolution, using distributed forcing. We used the same forcing data as Melsen et al. (2016a), where the data is interpolated using the pre-processing tool WINMET

20 of the PREVAH modelling system (Viviroli et al., 2009; Fundel and Zappa, 2011). For a more detailed explanation of the basin and the data used, we refer to Melsen et al. (2016a).

For this application, we focus on three sub-basins in the Thur to validate the model at three different spatial extents (see Fig 10a). We used a Monte Carlo approach to generate 25,000 parameter sets, with parameter boundaries based on the ranges presented in Fig. 8. We based the snow parameters on the study by Teuling et al. (2010). To capture the spread in parameters

25 as a result of equifinality, the 100 best runs based on the Kling-Gupta efficiency (KGE) are selected for each sub-basin. The resulting discharge time series are presented in Fig. 10b to Fig. 10d.

In Fig. 10b to Fig. 10d the simulated discharge is compared with the observed discharge for three different basins. The three basins are ordered from small to large. The simple dynamical systems approach has already been applied to the Rietholzbach, the smallest of the three basins in Fig. 10, by Teuling et al. (2010), but in a lumped fashion. We see that the distributed version

30 of this concept is able to correctly simulate the discharge in this basin, but also in the bigger basins. In the top left corner of each subplot, 4 performance statistics are presented based on the run with the highest Kling-Gupta efficiency: the Kling-Gupta efficiency (maxKGE), Pearson correlation coefficient (r), ratio of variability (α), and bias (β). The KGE value within brackets represents the Kling-Gupta efficiency without the routing module. These metrics show that there is no substantial
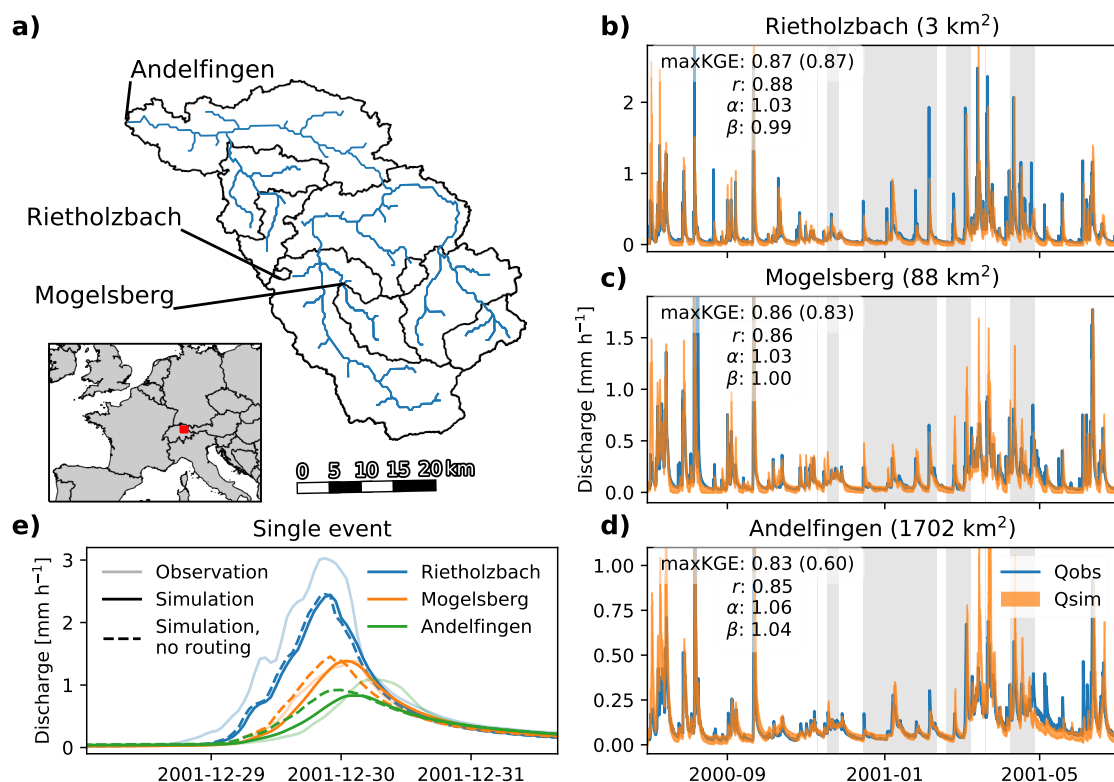
Figure 10. Application of dS2 to the Thur basin in Switzerland, where a) depicts the stream network and sub-basins used in this example. Graphs b) to d) present the model performance in three basins across different orders of sizes. The shaded orange region shows the minimum and maximum discharge of the selected best runs. Periods where more than 20% of the basin is covered with snow are indicated with the grey background. Graph e) shows how a single precipitation event is translated through the different (sub-)basins, where the light colours indicate the observed discharge, the dark lines represent the simulated discharge, and the dashed lines represent the simulated discharge without a delay induced by the routing module.

decrease in model performance with increasing catchment size. This indicates that the model is able to correctly simulate the discharge, independent of the catchment size. We do see, however, a clear decrease in the KGE values when no temporal delay is added via the routing scheme. In the smallest basin, both KGE values show the same result, yet in the largest basin, we see a substantial decrease in model performance. This indicates, in line with expectations, that the routing module is required to

5   optimally simulate larger basins.

To elaborate this, we zoom in to a single event in Fig. 10e. This graph shows the discharge response of the three sub-basins, and the effect of the routing module. For this event, we selected the parameter set from the 100 sets that performed best for this specific event. We see that, although the magnitude of the peak is not fully captured in the Rietholzbach and Andelfingen basins, the timing of the peak is well simulated in all three basins. The run without the routing module indicates that the impact

of the routing module depends on the size of the catchment, where the difference between these runs is largest in the biggest catchment. The differences between these runs explain the reduction in model performance in Fig. 10b to Fig. 10d, measured using the KGE without routing.

6 Discussion

5   As stated in the introduction, the aim of this paper is not to present the best or most comprehensive conceptual rainfall-runoff model, but to develop a model that can more easily be used to perform studies that require a large number of runs, such as uncertainty or sensitivity studies. As a result, this model concept has several limitations, either linked to the original simple dynamical systems approach or linked to the (distributed) implementation of this concept.

A limitation of the simple dynamical systems approach is that it assumes that the storage-discharge relation is the same in 10 the rising limb and in the falling limb of the hydrograph. Studies have shown that hysteresis exists in multiple basins, especially those dominated by a variable contributing area (Spence et al., 2010; Fovet et al., 2015). However, most common hydrological models do not explicitly account for hysteresis, and often struggle to correctly simulate the dry-to-wet transitions (de Boer-Euser et al., 2017). In our study, the simple dynamical systems approach assumes a fixed storage-discharge relation, with discharge being a function of only storage. In earlier studies where the concept was applied in a lumped fashion, this did not 15 limit the performance of the concept, especially in the studies where the $g(Q)$ parameters were retrieved from the discharge observations (Kirchner, 2009; Teuling et al., 2010). In our case study, this also did not seem to be a limiting factor. We do expect the model performance to be affected in basins with a strong hysteresis, yet we expect that one might define the $g(Q)$ function in a way that best captures the average behaviour of the rising and falling limbs.

Surface runoff as result of either infiltration excess or saturation excess are both not explicitly accounted for. Surface runoff 20 induced by over-saturated soils is implicitly accounted for in the discharge sensitivity function, which will reach high sensitivity values with high discharge (i.e. storage). During precipitation events with high intensity, surface runoff can also occur when the soil's infiltration capacity cannot meet the precipitation intensity. The model might therefore underestimate some discharge peaks resulting from infiltration excess overland flow. However, we expect that the influence of this process is minor in humid catchments. Not accounting for this process relates back to the purpose of this model, where we do not focus on correctly 25 representing catchments' internal fluxes, but instead focus on simulating the total discharge in a computationally efficient manner. It does, however, disqualify this concept for catchments with extreme precipitation events and the corresponding overland flow processes.

Furthermore, this model relies on the user to provide accurate evapotranspiration values as input for the model. As can be seen in Eq. (3), evaporation is directly taken into account in determining the change in storage. Due to the simplicity of 30 the concept, the model does not contain any evaporation reduction processes as result of e.g. soil moisture stress. The model disables evaporation when discharge drops below a threshold, behaving like an on-off switch, which is not how it is observed in reality. This reduction is most importantly preventing the model to calculate negative discharge values, while trying to behave like a real process.

The vectorized implementation limits the ability to transfer water between neighbouring pixels. This subsurface lateral flow is mostly driven by gravity, and is therefore expected to be most important in regions with large elevation differences. However, at the current recommend spatial-temporal scale of application (~ 1 km^2 and 1 h), we expect lateral subsurface flow to be relatively unimportant. At smaller spatial scales or longer time scales, flow between pixels can become more important.

5 To stay in line with the original scale of the simple dynamical systems approach, we do not recommend to further reduce the spatial resolution or to further increase the temporal resolution. Furthermore, most common hydrological models also do not account for flow between pixels (Liang et al., 1996; Arnold et al., 1998; Terink et al., 2015).

As proposed by Kirchner (2009), this concept can be used to "do hydrology backwards": infer precipitation from the discharge time series. Unfortunately, the distributed implementation of this concept complicates the use of this model to infer

10 spatially distributed rainfall maps. Since the resulting discharge is an average of the integrated catchment response, it is impossible to infer the location of the precipitation event. This will become especially difficult in large basins, where the time lag induced by routing will become larger. A study by Pan and Wood (2013) describes a method to infer precipitation from the stream flow observations, though it requires a relatively high number of observations. This method can potentially be applied to the model presented in this paper.

15 Finally, the current technical implementation of the model implies two other limitations. First, the routing scheme only induces a time lag on the discharge peak, and does not account for diffusion of the wave as it travels through the river network. For smaller basins, the effect of diffusion is only minor, but when simulating larger basins such as the Rhine, diffusion of the discharge wave will play a more important role. We recommend to use a more advanced routing scheme when applying the model to larger basins. The model can output a NetCDF file with runoff generated in each pixel per time step, which can

20 easily be connected to other routing software such as SOBEK. Secondly, the current version of the model does not (yet) support multi-threading, meaning that the model currently only runs on a single thread. Spreading the computational load over multiple threads is expected to further reduce the time required to run the model, especially in large basins. To make the model more efficient in single-thread mode, one can split the entire basin into several smaller sections and simultaneously run the model for each section. After the simulation is complete, the user can combine the several resulting pixel-wise runoff maps, and apply a

25 routing scheme on the entire basin.

7 Conclusions

The distributed simple dynamical systems (dS2) model is a new rainfall runoff model with the aim to simulate discharge in a computationally efficient manner. This model is based on the simple dynamical systems approach as proposed by Kirchner (2009), but has been modified to be applied in a distributed fashion, written in Python. In this way, the concept can be applied

30 to larger basins, while respecting the original spatial and temporal scale of the concept. We have extended the concept with a snow module and a simple routing module. The snow module can be turned on or off, depending on the basin of interest, and the routing module is required to transport water through the basin towards the outlet. The flexibility in the discharge sensitivity ($g(Q)$) function and the resulting strong non-linearity make this model different from more common "bucket-type" models.

As a result, dS2 is able to quickly simulate hydrological response at relatively high spatial ($\sim$1 km^2) and temporal ($\sim$1 hour) resolution.

Synthetic examples demonstrated that, although dS2 solves the water balance implicitly, the model is able to accurately close the water balance. The response surface plots for all parameter combinations show that there are some correlations

5   between the parameters, especially for the three discharge sensitivity parameters. However, we also showed that the parameters clearly influence different performance metrics, which provides the opportunity to reduce the calculation time of optimization algorithms. Finally, we have applied the model in the Thur basin as a case study to validate the performance of the model. Our model is able to correctly simulate discharge, both at the local scale (e.g. the Rietholzbach catchment in Switzerland, 3 km^2) and at the mesoscale (entire Thur basin in Switzerland, 1700 km^2), without a decrease in model performance as catchment size

10 increases.

The distributed simple dynamical systems (dS2) model has several unique strengths compared to other rainfall-runoff models: (1) it is computationally efficient even at high temporal and spatial resolutions, (2) it only has five parameters to calibrate, (3) two parameters have a clearly defined influence on the discharge time series making them easy to identify, and (4) the Python model code is open source and easily adjustable. The computational efficiency of this model creates the opportunity

15 to answer different research questions. Since the model is able to simulate regions in relatively short amounts of time, performing sensitivity and uncertainty analyses with a large number of samples becomes feasible. Since the model is distributed, the sensitivity and uncertainty analyses can be performed both on a spatial and temporal basis. Furthermore, this model can be a valuable tool for educational purposes, to explain and directly show the effects of modifying parameters in distinct groups (e.g. hydrological response, snow, routing, evaporation). Overall, this makes dS2 a valuable addition to the already large pool

20 of conceptual rainfall-runoff models, both for researchers as for practitioners interested in large sample studies.

Author contributions. JB, LAM and AJT conceived the idea behind dS2. JB developed the dS2 model, with valuable inputs from all co-

25 authors. JB performed the synthetic experiments and case study, LAM and AJT helped with interpreting the results. JB prepared the manuscript, with significant contributions from all co-authors.

Table A1. List of dS2 parameters

Name	Description	Example value	Unit
α	gQ parameter - intersect	-2.5	-
β	gQ parameter - slope	0.85	-
γ	gQ parameter - curvature	-0.010	-
ϵ	Reduction factor for evaporation	0.89	-
τ	Travel speed of water through the catchment	2	m s^{-1}
T0	Critical temperature	0	°C
ddf	Degree day factor for snowmelt	2	mm day^{-1} °C^{-1}
rdf	Conversion factor for energy to snowmelt	0.26	mm day^{-1} (W/m^2)$^{-1}$
Qt	Threshold below which evaporation is set to zero	10^{-4}	mm h^{-1}
dt	Size of time step (Δt)	1	h
max_RAM	Maximum RAM the model is allowed to use	1024	MB
size_one_value	Size of a single value	4	bytes
LB	Factor controlling lower boundary for solver, where $Q_t! \leq Q_{t-1} \cdot$ LB	10^{-4}	-
max_gQ_difference	Maximum allowed difference in gQ values	2	-
dt_reduction	Factor controlling the Δt reduction	0.15	-
min_extra_dt	Number of minimum extra Δt per Δt	5	-
max_extra_dt	Number of maximum extra Δt per Δt	50	-

References

Abramowitz, G.: Towards a Benchmark for Land Surface Models, Geophysical Research Letters, 32, https://doi.org/10.1029/2005GL024419, 2005.

Adamovic, M., Braud, I., Branger, F., and Kirchner, J. W.: Assessing the Simple Dynamical Systems Approach in a Medi-
5   terranean Context: Application to the Ardèche Catchment (France), Hydrology and Earth System Sciences, 19, 2427–2449, https://doi.org/https://doi.org/10.5194/hess-19-2427-2015, 2015.

Albergel, C., Dutra, E., Munier, S., Calvet, J.-C., Munoz-Sabater, J., de Rosnay, P., and Balsamo, G.: ERA-5 and ERA-Interim Driven ISBA Land Surface Model Simulations: Which One Performs Better?, Hydrology and Earth System Sciences, 22, 3515–3532, https://doi.org/https://doi.org/10.5194/hess-22-3515-2018, 2018.

10 Arnold, J. G., Srinivasan, R., Muttiah, R. S., and Williams, J. R.: Large Area Hydrologic Modeling and Assessment - Part 1: Model Development, Journal of the American Water Resources Association, 34, 73–89, https://doi.org/10.1111/j.1752-1688.1998.tb05961.x, 1998.

Best, M. J., Abramowitz, G., Johnson, H. R., Pitman, A. J., Balsamo, G., Boone, A., Cuntz, M., Decharme, B., Dirmeyer, P. A., Dong, J., Ek, M., Guo, Z., Haverd, V., van den Hurk, B. J. J., Nearing, G. S., Pak, B., Peters-Lidard, C., Santanello, J. A., Stevens, L., and Vuichard, N.: The Plumbing of Land Surface Models: Benchmarking Model Performance, Journal of Hydrometeorology, 16, 1425–1442,
15   https://doi.org/10.1175/JHM-D-14-0158.1, 2015.

Geoscientific
Model Development
Discussions

EGU

Beven, K.: Changing Ideas in Hydrology — The Case of Physically-Based Models, Journal of Hydrology, 105, 157–172, https://doi.org/10.1016/0022-1694(89)90101-7, 1989.

Beven, K.: How Far Can We Go in Distributed Hydrological Modelling?, Hydrol. Earth Syst. Sci., 5, 1–12, https://doi.org/10.5194/hess-5-1-2001, 2001.

5 Beven, K. J. and Kirkby, M. J.: A Physically Based, Variable Contributing Area Model of Basin Hydrology / Un Modèle à Base Physique de Zone d'appel Variable de l'hydrologie Du Bassin Versant, Hydrological Sciences Bulletin, 24, 43–69, https://doi.org/10.1080/02626667909491834, 1979.

Brauer, C. C., Teuling, A. J., Torfs, P. J. J. F., and Uijlenhoet, R.: Investigating Storage-Discharge Relations in a Lowland Catchment Using Hydrograph Fitting, Recession Analysis, and Soil Moisture Data, Water Resources Research, 49, 4257–4264,

10 https://doi.org/10.1002/wrcr.20320, 2013.

Brauer, C. C., Teuling, A. J., Torfs, P. J. J. F., and Uijlenhoet, R.: The Wageningen Lowland Runoff Simulator (WALRUS): A Lumped Rainfall–Runoff Model for Catchments with Shallow Groundwater, Geoscientific Model Development, 7, 2313–2332, https://doi.org/https://doi.org/10.5194/gmd-7-2313-2014, 2014.

Brutsaert, W. and Lopez, J. P.: Basin-Scale Geohydrologic Drought Flow Features of Riparian Aquifers in the Southern Great Plains, Water

15 Resources Research, 34, 233–240, https://doi.org/10.1029/97WR03068, 1998.

Buitink, J., Melsen, L. A., Kirchner, J. W., and Teuling, A. J.: The Distributed Simple Dynamical Systems (dS2) Model, https://doi.org/10.4121/uuid:cc8e0008-ab1f-43ee-b50d-24de01d2d0be, 2019.

Cash, J. R. and Karp, A. H.: A Variable Order Runge-Kutta Method for Initial Value Problems with Rapidly Varying Right-Hand Sides, ACM Trans. Math. Softw., 16, 201–222, https://doi.org/10.1145/79505.79507, 1990.

20 Clark, M. P., Slater, A. G., Rupp, D. E., Woods, R. A., Vrugt, J. A., Gupta, H. V., Wagener, T., and Hay, L. E.: Framework for Understanding Structural Errors (FUSE): A Modular Framework to Diagnose Differences between Hydrological Models, Water Resources Research, 44, https://doi.org/10.1029/2007WR006735, 2008.

Clark, M. P., Nijssen, B., Lundquist, J. D., Kavetski, D., Rupp, D. E., Woods, R. A., Freer, J. E., Gutmann, E. D., Wood, A. W., Brekke, L. D., Arnold, J. R., Gochis, D. J., and Rasmussen, R. M.: A Unified Approach for Process-Based Hydrologic Modeling: 1. Modeling Concept,

25 Water Resources Research, 51, 2498–2514, https://doi.org/10.1002/2015WR017198, 2015.

Comola, F., Schaefli, B., Ronco, P. D., Botter, G., Bavay, M., Rinaldo, A., and Lehning, M.: Scale-Dependent Effects of Solar Radiation Patterns on the Snow-Dominated Hydrologic Response, Geophysical Research Letters, 42, 3895–3902, https://doi.org/10.1002/2015GL064075, 2015.

Cornes, R. C., van der Schrier, G., van den Besselaar, E. J. M., and Jones, P. D.: An Ensemble Version of the E-OBS Temperature and

30 Precipitation Data Sets, Journal of Geophysical Research: Atmospheres, 123, 9391–9409, https://doi.org/10.1029/2017JD028200, 2018.

de Boer-Euser, T., Bouaziz, L., De Niel, J., Brauer, C., Dewals, B., Drogue, G., Fenicia, F., Grelier, B., Nossent, J., Pereira, F., Savenije, H., Thirel, G., and Willems, P.: Looking beyond General Metrics for Model Comparison – Lessons from an International Model Intercomparison Study, Hydrol. Earth Syst. Sci., 21, 423–440, https://doi.org/10.5194/hess-21-423-2017, 2017.

Fovet, O., Ruiz, L., Hrachowitz, M., Faucheux, M., and Gascuel-Odoux, C.: Hydrological Hysteresis and Its Value for

35 Assessing Process Consistency in Catchment Conceptual Models, Hydrology and Earth System Sciences, 19, 105–123, https://doi.org/https://doi.org/10.5194/hess-19-105-2015, 2015.

Fundel, F. and Zappa, M.: Hydrological Ensemble Forecasting in Mesoscale Catchments: Sensitivity to Initial Conditions and Value of Reforecasts, Water Resources Research, 47, https://doi.org/10.1029/2010WR009996, 2011.

Geoscientific
Model Development
Discussions

Huuskonen, A., Saltikoff, E., and Holleman, I.: The Operational Weather Radar Network in Europe, Bulletin of the American Meteorological Society, 95, 897–907, https://doi.org/10.1175/BAMS-D-12-00216.1, 2013.

Kirchner, J. W.: Catchments as Simple Dynamical Systems: Catchment Characterization, Rainfall-Runoff Modeling, and Doing Hydrology Backward, Water Resources Research, 45, https://doi.org/10.1029/2008WR006912, 2009.

5 Kirkby, M. J.: Tests of the Random Network Model, and Its Application to Basin Hydrology, Earth Surface Processes, 1, 197–212, https://doi.org/10.1002/esp.3290010302, 1976.

Koster, R. D. and Suarez, M. J.: Soil Moisture Memory in Climate Models, Journal of Hydrometeorology, 2, 558–570, https://doi.org/10.1175/1525-7541(2001)002<0558:SMMICM>2.0.CO;2, 2001.

Krier, R., Matgen, P., Goergen, K., Pfister, L., Hoffmann, L., Kirchner, J. W., Uhlenbrook, S., and Savenije, H. H. G.: Inferring Catchment
10 Precipitation by Doing Hydrology Backward: A Test in 24 Small and Mesoscale Catchments in Luxembourg, Water Resources Research, 48, W10 525, https://doi.org/10.1029/2011WR010657, 2012.

Kustas, W. P., Rango, A., and Uijlenhoet, R.: A Simple Energy Budget Algorithm for the Snowmelt Runoff Model, Water Resources Research, 30, 1515–1527, https://doi.org/10.1029/94WR00152, 1994.

Liang, X., Lettenmaier, D. P., Wood, E. F., and Burges, S. J.: A Simple Hydrologically Based Model of Land Surface Water and Energy
15 Fluxes for General Circulation Models, Journal of Geophysical Research, 99, 14 415–14 428, https://doi.org/10.1029/94JD00483, 1994.

Liang, X., Wood, E. F., and Lettenmaier, D. P.: Surface Soil Moisture Parameterization of the VIC-2L Model: Evaluation and Modification, Global and Planetary Change, 13, 195–206, https://doi.org/10.1016/0921-8181(95)00046-1, 1996.

Lindström, G., Johansson, B., Persson, M., Gardelin, M., and Bergström, S.: Development and Test of the Distributed HBV-96 Hydrological Model, Journal of Hydrology, 201, 272–288, https://doi.org/10.1016/S0022-1694(97)00041-3, 1997.

20 Liu, Y., Hejazi, M., Li, H., Zhang, X., and Leng, G.: A Hydrological Emulator for Global Applications – HE v1.0.0, Geoscientific Model Development, 11, 1077–1092, https://doi.org/https://doi.org/10.5194/gmd-11-1077-2018, 2018.

Lobligeois, F., Andréassian, V., Perrin, C., Tabary, P., and Loumagne, C.: When Does Higher Spatial Resolution Rainfall Information Improve Streamflow Simulation? An Evaluation Using 3620 Flood Events, Hydrology and Earth System Sciences, 18, 575–594, https://doi.org/10.5194/hess-18-575-2014, 2014.

25 Lyon, S. W. and Troch, P. A.: Hillslope Subsurface Flow Similarity: Real-World Tests of the Hillslope Péclet Number, Water Resources Research, 43, https://doi.org/10.1029/2006WR005323, 2007.

McDonnell, J. J., Sivapalan, M., Vaché, K., Dunn, S., Grant, G., Haggerty, R., Hinz, C., Hooper, R., Kirchner, J., Roderick, M. L., Selker, J., and Weiler, M.: Moving beyond Heterogeneity and Process Complexity: A New Vision for Watershed Hydrology, Water Resources Research, 43, W07 301, https://doi.org/10.1029/2006WR005467, 2007.

30 Melsen, L., Teuling, A., Torfs, P., Zappa, M., Mizukami, N., Clark, M., and Uijlenhoet, R.: Representation of Spatial and Temporal Variability in Large-Domain Hydrological Models: Case Study for a Mesoscale Pre-Alpine Basin, Hydrology and Earth System Sciences, 20, 2207–2226, https://doi.org/10.5194/hess-20-2207-2016, 2016a.

Melsen, L. A., Teuling, A. J., van Berkum, S. W., Torfs, P. J. J. F., and Uijlenhoet, R.: Catchments as Simple Dynamical Systems: A Case Study on Methods and Data Requirements for Parameter Identification, Water Resources Research, 50, 5577–5596,
35 https://doi.org/10.1002/2013WR014720, 2014.

Melsen, L. A., Teuling, A. J., Torfs, P. J. J. F., Uijlenhoet, R., Mizukami, N., and Clark, M. P.: HESS Opinions: The Need for Process-Based Evaluation of Large-Domain Hyper-Resolution Models, Hydrology and Earth System Sciences, 20, 1069–1079, https://doi.org/10.5194/hess-20-1069-2016, 2016b.

Pan, M. and Wood, E. F.: Inverse Streamflow Routing, Hydrol. Earth Syst. Sci., 17, 4577–4588, https://doi.org/10.5194/hess-17-4577-2013, 2013.

Rodríguez-Iturbe, I. and Valdes, J. B.: The geomorphologic structure of hydrologic response, Water Resources Research, 15, 1409–1420, https://doi.org/10.1029/WR015i006p01409, 1979.

5 Ruiz-Villanueva, V., Borga, M., Zoccatelli, D., Marchi, L., Gaume, E., and Ehret, U.: Extreme Flood Response to Short-Duration Convective Rainfall in South-West Germany, Hydrology and Earth System Sciences, 16, 1543–1559, https://doi.org/https://doi.org/10.5194/hess-16-1543-2012, 2012.

Rupp, D. E. and Selker, J. S.: On the Use of the Boussinesq Equation for Interpreting Recession Hydrographs from Sloping Aquifers, Water Resources Research, 42, https://doi.org/10.1029/2006WR005080, 2006.

10 Rupp, D. E. and Woods, R. A.: Increased Flexibility in Base Flow Modelling Using a Power Law Transmissivity Profile, Hydrological Processes, 22, 2667–2671, https://doi.org/10.1002/hyp.6863, 2008.

Saltelli, A.: Making Best Use of Model Evaluations to Compute Sensitivity Indices, Computer Physics Communications, 145, 280–297, https://doi.org/10.1016/S0010-4655(02)00280-1, 2002.

Saltelli, A., Annoni, P., Azzini, I., Campolongo, F., Ratto, M., and Tarantola, S.: Variance Based Sensitivity Analysis of
15 Model Output. Design and Estimator for the Total Sensitivity Index, Computer Physics Communications, 181, 259–270, https://doi.org/10.1016/j.cpc.2009.09.018, 2010.

Sivapalan, M.: Pattern, Process and Function: Elements of a Unified Theory of Hydrology at the Catchment Scale, Pattern, Process and Function: Elements of a Unified Theory of Hydrology at the Catchment Scale, in: Encyclopedia of Hydrological Sciences, Encyclopedia of Hydrological Sciences, John Wiley & Sons, Ltd, John Wiley & Sons, Ltd, https://doi.org/10.1002/0470848944.hsa012, 2006.

20 Sobol′, I. M.: Global Sensitivity Indices for Nonlinear Mathematical Models and Their Monte Carlo Estimates, Mathematics and Computers in Simulation, 55, 271–280, https://doi.org/10.1016/S0378-4754(00)00270-6, 2001.

Spence, C., Guan, X. J., Phillips, R., Hedstrom, N., Granger, R., and Reid, B.: Storage Dynamics and Streamflow in a Catchment with a Variable Contributing Area, Hydrological Processes, 24, 2209–2221, https://doi.org/10.1002/hyp.7492, 2010.

Sutanudjaja, E. H., van Beek, R., Wanders, N., Wada, Y., Bosmans, J. H. C., Drost, N., van der Ent, R. J., de Graaf, I. E. M., Hoch, J. M.,
25 de Jong, K., Karssenberg, D., López López, P., Peßenteiner, S., Schmitz, O., Straatsma, M. W., Vannametee, E., Wisser, D., and Bierkens, M. F. P.: PCR-GLOBWB 2: A 5 Arcmin Global Hydrological and Water Resources Model, Geoscientific Model Development, 11, 2429–2453, https://doi.org/https://doi.org/10.5194/gmd-11-2429-2018, 2018.

Tague, C. and Grant, G. E.: A Geological Framework for Interpreting the Low-Flow Regimes of Cascade Streams, Willamette River Basin, Oregon, Water Resources Research, 40, https://doi.org/10.1029/2003WR002629, 2004.

30 Terink, W., Lutz, A. F., Simons, G. W. H., Immerzeel, W. W., and Droogers, P.: SPHY v2.0: Spatial Processes in HYdrology, Geosci. Model Dev., 8, 2009–2034, https://doi.org/10.5194/gmd-8-2009-2015, 2015.

Teuling, A. J., Lehner, I., Kirchner, J. W., and Seneviratne, S. I.: Catchments as Simple Dynamical Systems: Experience from a Swiss Prealpine Catchment, Water Resources Research, 46, https://doi.org/10.1029/2009WR008777, 2010.

Troch, P. A., Troch, F. P. D., and Brutsaert, W.: Effective Water Table Depth to Describe Initial Conditions Prior to Storm Rainfall in Humid
35 Regions, Water Resources Research, 29, 427–434, https://doi.org/10.1029/92WR02087, 1993.

Troch, P. A., Paniconi, C., and van Loon, E. E.: Hillslope-Storage Boussinesq Model for Subsurface Flow and Variable Source Areas along Complex Hillslopes: 1. Formulation and Characteristic Response, Water Resources Research, 39, https://doi.org/10.1029/2002WR001728, 2003.

Viviroli, D., Zappa, M., Gurtz, J., and Weingartner, R.: An Introduction to the Hydrological Modelling System PREVAH and Its Pre- and Post-Processing-Tools, Environmental Modelling & Software, 24, 1209–1222, https://doi.org/10.1016/j.envsoft.2009.04.001, 2009.

Weiler, M. and Beven, K.: Do We Need a Community Hydrological Model?, Water Resources Research, 51, 7777–7784, https://doi.org/10.1002/2014WR016731, 2015.